

## THE NIGHT-SKY AT THE CALAR ALTO OBSERVATORY II: THE SKY AT THE NEAR INFRARED

S.F. SÁNCHEZ<sup>1</sup>, U. THIELE<sup>1</sup>, J. ACEITUNO<sup>1</sup>, D. CRISTOBAL<sup>2</sup>, J. PEREA<sup>3</sup>, J. ALVES<sup>1</sup>,  
*Draft version September 30, 2008*

### ABSTRACT

We present the characterization of additional properties of the night-sky at the Calar Alto observatory, following the study started in Sánchez et al. (2007), hereafter Paper I. We focus here on the night sky-brightness at the near-infrared, the telescope seeing, and the fraction of useful time at the observatory. For this study we have collected a large dataset comprising 7311 near-infrared images taken regularly along the last four years for the ALHAMBRA survey ( $J$ ,  $H$  and  $Ks$ -bands), together with a more reduced dataset of additional near-infrared images taken for the current study. In addition we collected the information derived by the meteorological station at the observatory during the last 10 years, together with the results from the cloud sensor for the last  $\sim 2$  years. We analyze the dependency of the near-infrared night sky-brightness with the airmass and the seasons, studying its origins and proposing a zenithal correction. A strong correlation is found between the night sky-brightness in the  $Ks$ -band and the air temperature, with a gradient of  $\sim -0.08$  mag per  $1^\circ$  C. The typical (darkest) night sky-brightness in the  $J$ ,  $H$  and  $Ks$ -band are 15.95 mag (16.95 mag), 13.99 mag (14.98 mag) and 12.39 mag (13.55 mag), respectively. These values have been derived for the first time for this observatory, showing that Calar Alto is as dark in the near-infrared as most of the other astronomical sites in the world that we could compare with. Only Mauna Kea is clearly darker in the  $Ks$ -band, but not only compared to Calar Alto but to any other observatory in the world. The typical telescope seeing and its distribution was derived on the basis of the FWHM of the stars detected in the considered near-infrared images. This value,  $\sim 1.0''$  when converted to the V-band, is only slightly larger than the atmospheric seeing measured at the same time by the seeing monitor,  $\sim 0.9''$ . Therefore, the effects different than the atmosphere produce a reduced degradation on the telescope seeing, of the order of  $\sim 10\%$ . Finally we estimate the fraction of useful time based on the relative humidity, gust wind speed and presence of clouds. This fraction,  $\sim 72\%$ , is very similar to the one derived in Paper I, based on the fraction of time when the extinction monitor is working.

*Subject headings:* Astronomical Phenomena and Seeing

### 1. INTRODUCTION

The night sky brightness in the optical and near-infrared, the number of clear nights, the seeing, transparency and photometric stability are some of the most important parameters that qualify a site for front-line ground-based astronomy. There is limited control over all these parameters, and only in the case of the sky brightness is it possible to keep it at its natural level by preventing light pollution from the immediate vicinity of the observatory. Previous to the installation of any observatory, extensive tests of these parameters are carried out in order to find the best locations, maximizing then the efficiency of these expensive infrastructures. However, most of these parameters are not constant along the time.

We have started a program to determine the actual values of the main observing conditions for the Calar Alto observatory. The Calar Alto observatory is located at 2168m height above the sea-level, in the Sierra de los Filabres (Almeria-Spain) at  $\sim 45$  km from the Mediterranean sea. It is the second largest European astronomical site in the north hemisphere, behind the Observatorio

del Roque de los Muchachos (La Palma), and the most important in the continental Europe. Currently there are six telescopes located in the complex, three of them operated by the Centro Astronómico Hispano Alemán A.I.E. (CSIC-MPG), including the 3.5m, the largest telescope in the continental Europe.

Along its 26 years of operations there has been different attempts to characterize some of the main properties described before: (i) Birkle et al. (1976) presented the first measurements of the seeing at Calar Alto, being the basis of the site testing; (ii) Leinert et al. (1995) determined the optical sky brightness corresponding to the year 1990; (iii) Hopp & Fernandez (2002) studied the extinction curve corresponding to the years 1986-2000; (iv) Ziad et al. (2005) estimated the median site seeing in the observatory from a single campaign in may 2002. A consistent study of all these properties was presented in Sánchez et al. (2007), including the first results of our program.

In that study, hereafter Paper I, we focused on the optical properties of the night sky, presenting (i) the first optical night-sky spectrum, identifying the natural and light pollution emission lines and their strength, (ii) the moon-less night-sky brightness in different optical bands, (iv) the extinction and its yearly evolution and (v) the atmospheric seeing and its yearly evolution. It was found that most of these properties were similar to those of major astronomical sites. In particular Calar Alto is among the darkest places in the world in the optical range.

Electronic address: sanchez@caha.es

<sup>1</sup> Centro Astronómico Hispano Alemán, Calar Alto, (CSIC-MPG), C/Jesús Durbán Remón 2-2, E-04004 Almeria, Spain

<sup>2</sup> Instituto de Astrofísica de Canarias, Vía Láctea S/N, La Laguna, S/C de Tenerife (Spain)

<sup>3</sup> Instituto de Astrofísica de Andalucía, Camino Bajo de Huétor S/N, Granada (Spain)

In the current study we focus on the near infrared (NIR) properties of the sky at Calar Alto. In particular we characterize here the typical and darkest sky brightness in the  $J$ ,  $H$  and  $K$ -bands, comparing them with similar properties in other observatories world-wide. Their dependencies with positioning in the sky and seasons are also analyzed. The typical seeing measured in real observations (telescope seeing) is derived and compared with the atmospheric seeing estimated by the seeing monitor (out of the telescope). Finally we estimate the fraction of useful time in the observatory based on the data obtained by the meteorological station along the last ten years (relative humidity and gust wind) and the presence of clouds based on the cloud sensor.

The structure of this article is as follows: in Section 2 we describe the dataset collected for the current study, including a description of data and the data reduction; in Section 3 we show the analysis and results performed over the different types of data and the results derived for each one; in Section 4 we summarize the main results and present the conclusions. All the magnitudes listed in this article are in the Vega system.

## 2. DESCRIPTION OF THE DATA

The main purpose of this study is the characterization of the sky brightness in the near infrared at the Calar Alto observatory. In order to address this goal we collected different observational data, taken with different telescopes and instruments and using different methods to calibrate, reduce and analyze the data. With this selection we try to minimize the effects on the results of a particular instrumental setup, maximizing the reliability of the dataset and its time coverage.

### 2.1. Observations of Calibration Stars

As we indicated in detail in Paper I the most obvious method to derive the sky brightness is to obtain direct imaging on calibration stars (or well calibrated fields), using the well known photometry of the observed stars to self-calibrate the images and then derive the sky surface brightness. With this purpose, observations were taken using the MAGIC NIR camera (Herbst et al. 1993) at the 1.23m telescope during the nights of the 30th and 31st of January 2008. Although a strong dependency of the NIR sky brightness with the moon (at least for the  $H$  and  $K$  bands) is not expected, both nights were selected to be dark. In both nights we used the  $J$ ,  $H$ ,  $K_s$ ,  $K$  and  $K_m$  bands. The MAGIC detector is an Rockwell NICMOS3 array of  $256 \times 256$  pixels, with a scale of  $1.2''/\text{pixel}$  and a field-of-view of  $5.1' \times 5.1'$ , enough for the purpose of this study. MAGIC is under operation at Calar Alto since 1995, and it is not in regular use anymore.

On the 30th of January we observed the core of M67, taking 24 individual frames of 60s per band (splitted in individual integrations of 2s each one). This cluster was selected since there are publically available NIR photometry for most of its members and on the indicated date it remains near the zenith (airmass < 1.2) during most of the night. On the 31st we took 24 individual frames of 60s per band on a single calibration star from the UKIRT faint photometric standards (Casali & Hawarden 1992), observing it at different airmasses. In both nights the observations were started two hours after the twilight, in order to minimize as maximum its possible effects (if any).

The data were reduced following standard procedures for the near infrared, using IRAF (Tody 1993)<sup>4</sup> and self programmed routines. Each frame was corrected by its corresponding dark frame and flatfielded using flux normalized domeflats. Bad pixels were identified using both the dark and the domeflats and masked from the individual frames. Since we are interested in the sky brightness no sky subtraction was applied.

Once the images were reduced we measured the number of counts within an aperture of  $8''$  for the brightest stars detected in the field (in the case of the 30th of January data) or the photometric standard (in the case of the 31st of January data). The number of counts from the sky was determined by measuring it directly in an annular ring of  $14''$  and  $27''$  (inner and outer radii). After subtracting the sky to the counts of the detected stars the photometric zeropoint for the image was determined using the formula:

$$\text{mag}_{\text{zero}} = \text{mag}_{\text{app}} + \text{ext} + 2.5 \log_{10}(\text{counts}/t_{\text{exp}}) \quad (1)$$

where  $\text{mag}_{\text{zero}}$  is the magnitude zeropoint,  $\text{mag}_{\text{app}}$  is the apparent magnitude of the calibration star in the corresponding band, “ext” is the extinction, “counts” are the measured counts within the indicated aperture, and  $t_{\text{exp}}$  is the exposure time. When more than one star was analyzed we adopted the mean value of the derived zeropoints as the image photometric zeropoint. After that the surface sky-brightness was derived for each image by using the formula:

$$\text{SB}_{\text{sky}} = \text{mag}_{\text{zero}} - 2.5 \log_{10}(\text{counts}_{\text{sky}}/t_{\text{exp}}/\text{scale}^2) \quad (2)$$

where  $\text{SB}_{\text{sky}}$  is the surface brightness in magnitudes per square arcsec,  $\text{mag}_{\text{zero}}$  is the zeropoint described before,  $\text{counts}_{\text{sky}}$  is the sky counts level estimated and “scale” is the pixel scale in arcseconds. It is noticed that the magnitude zeropoint was corrected by the extinction, but the sky brightness was not, following the convention adopted in most of the recent studies of sky brightness (Paper I and references therein). Correcting the sky brightness for extinction would be appropriate only if the extinguishing layer were known to be below all sources of sky brightness, which is not the case (Benn & Ellison 1998a,b).

For the extinction we used the formulae presented in Paper I, that allows to estimate the extinction in the NIR bands based on the  $V$ -band extinction from the Calar Alto Extinction Monitor (CAVEX, PI: U.Thiele, see Paper I). In both nights the extinction in the NIR was almost neglectible. We finally got 24 individual estimations of the surface sky brightness for each band and night.

### 2.2. Observations of the ALHAMBRA survey

The ALHAMBRA survey (Moles et al. 2008) is the largest cosmological survey currently on going at the Calar Alto Observatory. It comprises the observation of 4 discontinuous square degrees on the sky in 8 different locations using 20 middle-width filters in the optical

<sup>4</sup> IRAF is distributed by the National Optical Astronomy Observatories, which are operated by the Association of Universities for Research in Astronomy, Inc., under cooperative agreement with the National Science Foundation.

range and three additional ones (J, H and Ks) in the near infrared. The locations were selected to cover areas of low galactic extinction, without very bright stars in the field, and/or corresponding areas already covered by other extragalactic surveys (like COSMOS, HDFN or the GROTH-strip). The main goal of this survey is to derive high quality photometric redshift of about  $\sim 1.6$  million of galaxies, in order to study the evolution of galaxies up to  $z \sim 1$ . The NIR observations of the survey are taken with the Omega2000 camera mounted in the 3.5m telescope at Calar Alto. This camera has installed a Hawaii-2 detector with an array of  $2048 \times 2048$  pixels, each one with projected size of  $0.447''$ . Thus, the detector covers a field-of-view of  $\sim 15' \times 15'$ . Omega2000 is under operations at Calar Alto since 2001, and it has been for a long period of time one of the NIR cameras with the largest field-of-view in the world. To observe the proposed field-of-view and to achieve the proposed depth ( $Ks < 20$  mag,  $5\sigma$  detection limit) the ALHAMBRA survey obtains several individual frames of 80s (J), 60s (H) and 46s (Ks) each one, at many different locations on the sky, being an unique dataset to study the properties of the NIR sky brightness (as an unproposed legacy).

The ALHAMBRA survey has accumulated observations with Omega2000 along 75 nights, from August 2004 to March 2008, with about  $\sim 150$  individual frames per night. That means about  $\sim 3500$  individual frames on target per band. These nights corresponds to a  $\sim 67\%$  of the allocated nights for the project in that time interval, which reinforces our claim in Paper I that a  $\sim 70\%$  of the nights are useful for astronomical observations at Calar Alto (see Section 3.3 for a full discussion).

To automate and homogenize the data reduction a semiautomatic pipeline was created (Cristobal et al. 2008, in prep.). This pipeline performs the typical reduction steps for NIR imaging data, including the dark-current subtraction, flat-fielding, image combination, sky determination and subtraction and flux calibration. The flux calibration was performed self-calibrating the images using the NIR magnitudes of the field stars extracted from the 2MASS survey (Skrutskie et al. 2006). The typical error of the magnitudes of each individual star is about  $\sim 0.03$  mag, with a range of errors between  $\sim 0.02$  and  $\sim 0.10$  mag. The large field-of-view of Omega2000 grants the detection of a sufficiently large number of them ( $> 20$ ) to obtain an accurate flux calibration, better than  $\sim 0.025$  mags (Cristobal et al., in prep.). As a by product of the pipeline the sky background is determined for each combined image.

Due to its nature the different pointings of the survey are observed in different nights, at different azimuths and elevations (and airmasses). Therefore, the derived sky backgrounds from the combined frames cannot be used to characterize particular nights and/or atmospheric conditions. However, they are still useful indicators of the average sky background in the observatory.

For the present study we collected the night sky backgrounds available from the ALHAMBRA reduced dataset, all of them corresponding to 12 different nights of the same month, August 2004 (the 1st run of the survey). These data have the advantage of their high signal-to-noise, due to the depth of the combined images, and the fact that they have been reduced using a refined pipeline. The final sample comprising a set of 17

individual estimations of the sky background per filter.

A simpler procedure was developed to obtain the sky brightness for each individual frame obtained by the survey, which comprises a much larger dataset. For each individual frame taken on the ALHAMBRA fields the approximate location of the field stars with NIR magnitudes derived by the 2MASS survey were obtained. Poststamp images with a field-of-view of  $40'' \times 40''$  around these locations were taken. In each individual poststamp the location of the field star was determined by a simple centroid determination, masking the pixels up to  $5\sigma$  the standard deviation over the median background. Then, the counts within an aperture of  $6''$  radius around the determined centroid were measured, subtracting the background counts estimated within a ring between  $14''$  and  $20''$  radius and the nominal dark-current of the instrument (Kovács et al. 2004). Simultaneously the median counts within four different boxes of  $18 \times 18$  pixels located at  $10''$  away from each centroid was derived as an estimation of the counts of the sky brightness. The estimated counts per star were used to derive a magnitude zero-point for each star in the field with known photometry using the formulae (1), and the corresponding sky surface brightness using formulae (2) and the estimation of the sky counts. The number of stars detected per field with accurate 2MASS photometry grants the quality of the derived surface sky-brightness, despite the fact that the accuracy of the individual photometry is not that good in a few cases, as indicated before. The fact that no flat-field correction was applied should not affect strongly the results due to the small variations in the efficiency pixel-to-pixel in the Omega2000 array.

We finally got a sample of 1954, 2394 and 2963 individual estimations of the night sky surface brightness for the J, H and Ks bands. Due to the number of measurements and the time coverage it comprises one of the largest samples of this nature ever obtained to our knowledge.

As a by-product of the analysis it was derived the average FWHM on each analyzed image. For doing so it was extracted an horizontal and vertical intensity cut along and across the estimated centroid in each poststamp image. The intensity cuts were then fitted with a single gaussian function plus a continuum intensity to remove the background. The average of the horizontal and vertical FWHMs is taken as the FWHM of the image of each star, and then, the median value of the FWHMs derived on the same image is stored. Once removed the effect of the pixel scale, the final FWHM can be considered as the seeing in the detector plane in the considered band.

A summary of all the data set collected for this study is listed in Table 1, including the date of the observations or the projects from where they were extracted, the telescope and instrument used, the bands covered by the data and the number of individual frames analyzed (the number of individual sky background estimations).

### 2.3. Meteorological conditions

The atmospheric conditions in the observatory has been continuously monitored by a computerized meteorological station during the last decade. This station measures the most important meteorological parameters, such as the surface temperature, the relative humidity, the wind speed and direction, the wind gust speed and

the air pressure, and store it every 30 seconds. These data comprises a huge dataset with 3541161 individual measurements of each parameter for the time period between January 1998 and December 2008, that allows to characterize the atmospheric conditions at Calar Alto.

### 3. ANALYSIS AND RESULTS

#### 3.1. *The typical Night Sky Brightness at the near infrared*

The near infrared sky brightness is dominated by many intricately narrow hydroxyl (OH) emission lines (eg., Oliva & Origlia 1992; Rousselot et al. 2000; Cox 2000). A few other species (eg., molecular oxygen at 1.27  $\mu\text{m}$ ) also contribute, as do  $\text{H}_2\text{O}$  lines at the long wavelength end of the *K*-bands. Another contributions to the sky background is zodiacal emission (eg., Harwit et al. 1969; Content 1996; Cox 2000), thermal emission from the atmosphere and the telescope (which follows a graybody curve, Content 1996), and the moonlight (eg., Cox 2000).

All these effects contributes differently at different wavelength ranges. In the *J*-band the moon-light may have a strong effect, if it is observed near the moon. On the other hand, its effect is neglectible in the *H* and *K*. In general, the dominant effect in the *J* and *H* bands is the OH emission lines, although the effect of the zodiacal light is not neglectible, being similar in both bands (eg., Content 1996). However, in the *K*-band the thermal emission becomes the dominant effect, in particular the telescope one (eg., Cox 2000), being less important the OH emission lines, and the optical airglow is almost neglectible.

The night sky brightness suffers strong variations along each night which impose limitations to the concept of *typical* sky brightness. The OH emission varies diurnally, being stronger in the daytime and at twilight. It may decrease by a factor 2 or 3 in one or two hours after the twilight, and it does not increase again just before the sunrise. Its emission roughly scales with the airmass, which produces an increase of the sky brightness at higher airmasses, especially in the *J* and *H* bands.

The variation in the night sky brightness due to all these effects can be appreciated in Figure 1. This figure shows all the individual night sky surface brightnesses that comprise the dataset derived from the ALHAMBRA survey (described before), along the Universal Time corresponding to each of the 75 observed nights. The wider range of surface brightness it is found in the *Ks*-band, while the narrower one corresponds to the *J*-band.

As a rough estimation of the typical sky brightness it was derived the median sky brightness of each dataset. For a better characterization it was also derived the darkest sky brightness and the brightest one, which will illustrate the strength of the variation of the sky brightness. For the full sample of the ALHAMBRA dataset, which includes data taken at many different epochs this latter parameter were not derived, since it turns to be meaningless. All these estimations of the sky brightness are listed in Table 2, for each data-set and each band.

The values listed in the table illustrate how strong is the variation of the sky brightness, not only within a certain night, but also night-to-night. In this context the median sky brightness is the less useful parameter to characterize the sky brightness, since it was included in its derivation data taken at different times from the

twilight and at different airmasses. A good example of the biases that can be found by adopting the median sky brightness are the data of the two nights observed at the 1.23m telescope. They correspond to observations on two consecutive nights, using the same instrument at the same telescope. However, there is a strong difference in the median sky brightness derived for each of these nights, at least for the *J* and *H* bands. As we will show later the main reason for these differences is due to the air-mass range of the observations taken each night. While the 1st night the observations were restricted almost to the zenith ( $X < 1.2$ ), in the second one it was explored a wide range of airmasses. This may explain also the strong differences found among the brightest sky brightness for the same bands for the different datasets.

A more reliable parameter to characterize the sky brightness is the darkest sky brightness derived for each band in the different datasets. Although this parameter also presents a variation, this is much reduced than the one found in the median sky brightness. However it does not illustrate the expected sky brightness at the observatory in any conditions, it just represents the darkest ever possible sky that can be found on the data set. As expected the darkest sky-brightness is found in the largest dataset, since it covers the wider range of atmospheric conditions, and therefore it has the largest probability of catching the optimal ones.

##### 3.1.1. *Dependency on the zenith distance*

As indicated before the sky brightness presents a dependency with the zenith distance. In the optical range this dependency is mostly due to the airglow, an effect that is stronger at largest airmasses and smaller at the zenith (eg., Paper I and references therein). In the NIR there are additional components that depend mostly on the OH emission (and the thermal emission), and which effect is minimized also at the zenith.

In general the dependency of the sky brightness with the airmass (ie., the zenith distance) can be modeled by the following formula:

$$\Delta m = -2.5 \log_{10}[(1-f) + fX] + \kappa(X-1)$$

The first two parameters within the logarithm of this formula are described in Patat (2003), being  $\Delta m$  the increase in sky brightness at a certain band and airmass ( $X$ ),  $f$  the fraction of the total sky brightness generated by airglow, and  $(1-f)$  the fraction produced outside the atmosphere (hence including zodiacal light, faint stars and galaxies). Finally,  $\kappa$  is the extinction coefficient at the corresponding wavelength. As already indicated in Paper I these two parameters describe correctly the dependency of the sky brightness with the airmass for the optical range. Indeed the fraction  $f$  is almost constant for the optical range, being of the order of  $\sim 0.6$  (eg., Benn & Ellinson 1998a,b). However in the near-infrared the fraction of night sky light generated in the atmosphere can be larger than the one generated outside the atmosphere, and therefore “ $f$ ” can be larger than 1.

This formula is an approximation for low airmasses of the so-called van Rhijn formula (eg., Chamberlain 1961), which describe the increase of the airglow emission when the zenith angle increases. The extinction correction has to be taken into account since the light, emitted in a

layer on top of the atmosphere, is attenuated by the atmospheric extinction.

Figure 2 shows the distribution of the NIR surface sky brightness along the airmass for the different bands observed in the night of the 31st of January 2008. As expected, there is a clear dependency of the surface brightness with the airmass, particularly strong in the  $J$  and  $H$  bands. A similar result is found in any night within our different collected dataset. This particular night was shown just as an illustrative example, since its dataset covers the larger number of filters and a wide range of airmasses.

The sky-brightness/air-mass distribution derived for each night and filter were fitted with the parametrization described before. For the  $J$  and  $H$  band it was obtained that a value of  $f \sim 2.6$  reproduces well the air-mass dependency of the night sky brightness. The similarities between both bands are mostly due to the fact that the sky brightness is dominated in both of them by very intense OH bands. The  $J$ -band covers the 7-4 and 8-5 OH bands, while the  $H$ -band covers the 4-2, 5-3 and 6-4 ones (eg., Chamberlain 1961; Maihara et al. 1993; Leinert et al. 1998). On the other hand, the air-mass dependency is weaker in the  $K$ -band. A “ $f$ ” value of  $\sim 0.4$  reproduces well its shape. The  $K$ -band is less affected by the OH bands. Only a part of the 9-7 band enters at wavelengths lower than  $2.2\mu\text{m}$ , and there is wide gap without any OH band between  $2.2\mu\text{m}$  and  $2.7\mu\text{m}$  (eg., Leinert et al. 1998). For this band the thermal contribution starts to be important (eg., Content 1996; Leinert et al. 1998; Glass 1999).

### 3.1.2. The sky brightness at the Zenith

The results from the parametrization shown in the previous section were used to correct the sky-brightness from its dependency with the airmass and to transform all the measured values to the corresponding value at the zenith. As already indicated in Paper I, and references therein, these values are a good characterization of the typical sky-brightness for an astronomical site.

Table 3 lists the median sky-brightness for the different considered bands after applying the considered correction for the dataset corresponding to the full sample of ALHAMBRA data. In addition it is listed the median values of the uncorrected sky-brightnesses restricted to the airmasses near to the zenith ( $X < 1.05$ ) for the considered dataset. Although this later is a much limited sample ( $\sim 150$  measurements), the good agreement between both estimations of the zenithal sky-brightness, within  $\sim 0.1$  mag, reinforces the validity of the adopted correction.

In order to test the effects of the thermal emission on the sky-brightness the data were splitted in two subsamples, one covering the colder epoch of the year (from November to February, so called *winter*), and another comprising the rest of the year (so called *summer*). The median zenithal sky-brightness were derived for both datasets and listed in Table 3. Only in the  $Ks$ -band is appreciated a clear seasonal difference, with the winter sky-brightness being  $\sim 0.8$  mags darker than the summer one, on average. These differences in the sky brightness along the year are clearly appreciated in Figure 3, where the median zenithal sky-brightness for each night and filter are represented along the year. Again, only for the

$Ks$ -band the sky-brightness shows a clear pattern, with a change associated with the seasons, being brighter in the summer and darker in the winter. This result is consistent with the expected origin of the sky-brightness at the different bands, since the thermal contribution should affect strongly the  $Ks$ -band.

To investigate the actual dependency of the  $Ks$ -band sky-brightness with the temperature we derived the average air temperature measured by the meteorological station for the nights with measured sky-brightness, comparing both parameters. In Figure 4 it is shown the distribution of the average, air-mass corrected, sky brightness for the  $J$ ,  $H$  and  $Ks$ -band along the average temperature for the considered nights. As expected there is a clear dependency of the sky brightness with the temperature (with a correlation coefficient of  $r = 0.88$ ), only for the  $Ks$ -band data. A linear regression derives an increase of  $\sim 0.08$  mag in the sky brightness per  $1^\circ$  increase in temperature. The temperature at Calar Alto presents a seasonal sinusoidal pattern, with a minimum in winter (December-January) at  $\sim -8^\circ$  C and a maximum in summer (July-August) at  $\sim 12^\circ$  C. Due to this thermal variance it should be possible to find differences in the sky brightness of  $\sim 2$  mag between the coldest nights in winter and the hottest in summer.

It has been long suspected that the thermal background in the 3.5m telescope is larger than in rest of the telescopes at Calar Alto, due to its larger structure. However this claim has never been tested. Although we do not have a similar sample of sky-backgrounds measured in the rest of the telescopes, the fact that the  $Ks$ -band background correlates so tightly with the atmospheric temperature make us to suspect that this claim is not correct. Indeed, the two estimations of the sky-brightness taken at the 1.23m, marked with two big circles in Figure 4 lie exactly in between the remaining data, taken at the 3.5m telescope.

### 3.1.3. Comparison with other astronomical sites

As indicated in the introduction the night sky-brightness is a fundamental parameter to estimate the quality of a certain astronomical site. A fair comparison of this parameter among different observatories is the best method to establish their real status. In order to perform this exercise we collected all the published estimations of the night sky-brightness available in the literature and in the observatories webpages at different sites. The result from this collection is listed in Table 4, including the name of the observatory where the data were obtained, the kind of measurement listed (average or darkest sky brightness), the measured sky-brightness for the  $J$ ,  $H$  and  $Ks$ -bands and the reference from where the data were extracted.

To perform a fair comparison between the sky brightness at these different sites and Calar Alto it is required to use the same kind of measurement. For the darkest sky brightness we will use the corresponding values listed in Table 3, and for the average ones we will use those listed in Table 2. In some cases, like in Cerron Pachon and Mt.Graham, it is not clearly stated in the references if they correspond to the average or the darkest sky brightness. We adopted the less advantage situation for Calar Alto for the purposed comparison and consider their measurements as the average (that is al-

ways brighter) instead of the darkest.

Regarding the darkest sky-brightness it is clear that for the  $J$  (16.96 mag) and  $H$ -bands (14.98 mag) Calar Alto can be quoted among the darkest astronomical sites in the world (or at least the ones listed here). For the  $Ks$  band (13.55 mag) its sky-brightness is clearly comparable with most of the astronomical sites, apart from Mauna Kea, which is, by far, the darkest place for this considered wavelength range. This is expected since this site is located by far at the highest altitude, as it is seeing in Table 4, with the most tenuous atmosphere, and therefore the thermal background there is much lower than in any of the other sites.

For the average sky-brightness we can only compare with the published sky-brightnesses from el Roque de los Muchachos observatory at La Palma island and Mauna Kea. In the  $J$ -band Calar Alto seems to be darker than La Palma or Mauna Kea by  $\sim 0.3$  mag and in the  $H$ -band the three places seem to be equally dark. On the other hand, in the  $Ks$ -band Calar Alto is slightly brighter than La Palma, by  $\sim 0.2$  mag, and both places are much brighter than Mauna Kea, by  $\sim 1$  mag, as expected. However, considering the inhomogeneity of the collected data and the lack of details of how they were derived we consider that only the differences found with Mauna Kea in the  $Ks$ -band are really significative.

### 3.2. The seeing measured at the detector

In Paper I we published the median site seeing at the Calar Alto observatory estimated from a continuous night monitoring of the atmospheric seeing performed with a DIMM monitor since August 2004 (RoboDIMM, PI: J.Aceituno). However it is well known that the site seeing is not in most cases the actual seeing measured in the detector when an astronomical image is taken. There are several reasons for this effect, being the stronger ones:

- The Dome seeing. The turbulence created by the temperature differences between the air inside the dome and outside the dome creates a local seeing. For that reason modern telescopes are build with smaller domes or domes that open wider than traditional telescopes. In this regards the large domes of the equatorial mounted telescopes at Calar Alto are clearly a handicap which in principle could create bad dome seeings. In the last years there has been a large upgrade in the domes at Calar Alto. New windows were opened in the dome and large fan systems were installed to create laminar airflows that cool down the dome and reduce the turbulence, in order to limit the effects on the seeing.
- The mirror seeing. The differences between the temperature on the dome and the surface of the primary mirror creates turbulence in its vicinity that alters the measured seeing. Due to its larger thermal capacity, mirrors are cooled down slower than the dome, and therefore this effect may affect a sustantial fraction of the astronomical night. To reduce this effect it was installed a cooling system that pumps evaporated nitrogen to the primary mirror while the telescope is parked during the day, reducing the thermal gradient and its effect over the seeing.

- Optical problems with the telescope, like bad focusing, misalignments of the primary and secondary mirror (or prime-focus instrument), astigmatig effects.
- Mechanical or electronical problems like bad balancing (that creates vibrations and fleasures), tracking and/or guiding problems.

For all these reasons it is interesting to estimate the seeing measured in the astronomical images and compare it with the site seeing to estimate the quality not only of the observatory but also of the telescopes installed on it.

For doing so we used the seeing estimated for each frame of the full ALHAMBRA survey dataset, described in Section 2.2. It is known that the seeing presents a strong wavelength dependency, being smaller in the red-der bands than in the bluer ones. To perform a fair comparison with the site seeing measured by the DIMM at the  $V$ -band it is required to transform the estimated seeing at each NIR band to the former one. For doing so we adopted the transformation derived by Sarazin & Roddier (1990):

$$\text{Seeing}_\lambda = \text{Seeing}_{\lambda_0} \left( \frac{\lambda}{\lambda_0} \right)^{-0.2}$$

After applying this transformation its was obtained a final sample of 7311 individual seeing estimations on the detector at the  $V$ -band that can be directly compared with the site seeing measured by the seeing monitor. Figure 5 shows the distribution of the seeing measured directly at the detector together with the distribution of the site seeing measured by the DIMM monitor in the same time period. As expected the former distribution has an offset towards larger seeings than the previous one, but there is no evidence of a broader tail. This indicates that although the telescope seeing is worst than the site one, there is little evidence of disastrous seeings. The stronger contribution to the seeing at the detector is site one, and not the remaining effects described before.

The median seeing measured at the detector is  $\sim 1.0''$  (converted to the  $V$ -band), while the site seeing is  $\sim 0.9''$  for the same time period, with a standard deviation of  $\sim 0.2''$  in both cases. Therefore, the added degradation of the seeing due to the technical characteristics of the telescope/instrument is statistically restricted to  $\sim 10\%$  of the site seeing value. For comparison purposes the measured seeing distribution in the  $Ks$ -band is also shown in Fig. 5 (dash-dotted line). The median seeing in this band is  $\sim 0.77''$ , with a standard deviation of  $\sim 0.13''$ . A  $\sim 50\%$  of the nights the seeing is lower than this typical value.

### 3.3. The Fraction of useful time

A fundamental parameter to estimate the quality of a certain astronomical site is the fraction of time that it is possible to observe. This concept is always relative to the instrumentation/telescopes installed in the considered observatory. For example, radio telescopes can operate both during night and day time, while optical ones can only operate during the so-called astronomical night. In this regards the fraction of useful time has to be computed differently for different telescopes.

The telescopes at Calar Alto were designed to operate in a wide range of atmospheric conditions. In general they can operate with relative humidities down to a 95% and wind gust velocities down to 20 m/s. In certain conditions of temperatures, cloud coverage and atmospheric pressure they can still operate with relative humidities as high as a 98% and wind gust velocities as high as 26 m/s (at least the 3.5m telescope). Therefore the former limit is a conservative one to define when it is possible to observe.

The fraction of useful time was estimated for each night using the database of atmospheric parameters described in section 2.3, and adopting the definition of useful time as that time when the telescopes can operate, on the basis of the conservative limit described before. For the decade comprised in the dataset it was found that it was possible to observe in a  $\sim 72\%$  of the night time, and in a  $\sim 41\%$  of the nights the atmospheric conditions allows to observe for the full night. This estimation agrees with the fraction of useful time derived on the basis of the data from the extinction monitor described in Paper I.

Of the two parameters that define the adopted limit, the humidity is the more critical one since only in very rare cases a wind gust speed of 20 m/s is reached. Figure 6 shows the distribution of nightly average relative humidity along the time period sampled by the meteorological station. There is a clear seasonal pattern, with dry and more stable summers and wet and more instable winters. The peaks of high relative humidity in winter are due to low altitude clouds and rain. However, the driest periods are also present in winter, although less frequently and stable than in summer. These periods are due to freezing temperatures that dries the atmosphere. This pattern is reflected in the fraction of useful time, that in summer is  $\sim 85\%$  in average while in winter drops to a  $\sim 55\%$ .

This estimation has the caveat that in certain conditions it is still possible to have a covered sky by clouds while the humidity is lower than a 95%. With these conditions it will be possible to observe or not depending on the thickness of the clouds. In these cases the extinction measured by the extinction monitor is a good estimation of the it is possible to observe or not. However, as we indicated before there is no big differences between the fraction of useful times derived by the analysis of the atmospheric conditions and by the measurements of the extinction.

In order to quantify the presence of clouds it was installed in the observatory a cloud sensor in October 2006. This monitor determines the presence of clouds by estimating the difference in temperature between the sky and the ground, on the basis of the infrared emission of the former one<sup>5</sup>. This instrument is monitoring this temperature every minute since it become operational, which provides us with a sample of 466142 individual estimations of this parameter. Although it does not distinguish between thick and thin clouds, it is possible to establish when the sky completely covered, that it is when the sky is less than 15° C colder than the ground. By imposing this additional limitation to our adopted definition of useful time its actual fraction drops to a  $\sim 68\%$ . It is interesting to note here that this fraction is very similar

to the fraction of useful time derived directly from the observations of the ALHAMBRA survey (Section 2.2).

We conclude that the fraction of nights with low humidity and calm wind and covered by clouds is rather small.

#### 4. CONCLUSIONS

In this article we have continued the characterization of the main properties of the night-sky at the Calar Alto observatory that we started in Paper I. These properties were compared with similar ones of other different astronomical sites. The main results of this article can be summarized in the following points:

- The night sky brightness at the near-infrared presents a strong airmass dependency in the *J* and *H* band, and a mild one in the *Ks*-band. These dependencies can be modelled and corrected (or predicted) for any night and airmass by assuming that they are due to airmass dependency of the OH lines emission. Obviously, *J* and *H*-band observations are recommended to be performed near the zenith, while at the *Ks*-band this is less critical. This result should be taken into account when defining observing strategies in the future.
- There is a seasonal pattern in the *Ks*-band sky brightness, which shows an average difference of  $\sim 0.8$  mag from summer, when is brighter, to winter, when is darker. This pattern is due to the strong dependency of the sky-brightness in this band with the atmospheric temperature, which may indicate that the contribution from the thermal background emission is the dominant component in this band.
- The brightness of the night sky at Calar Alto is similar or darker than any in other major astronomical site in the *J* and *H* bands, including both Paranal and Mauna Kea. In the *Ks*-band all the astronomical sites are very similar apart from Mauna Kea, which is clearly darker (by  $\sim 1$  mag). Indeed, Calar Alto has a similar sky brightness than Paranal or La Palma at this wavelength range.
- The seeing on the detector is only slightly larger than the site seeing measured by the DIMM, outside the dome (at least for the 3.5m telescope). The effects different than the purely atmospheric ones produce a statistical increase of a  $\sim 10\%$  in the measured seeing on the detector compared with the site one.
- The fraction of useful time at the observatory is of the order of  $\sim 70\%$ , with  $\sim 40\%$  of the nights 100% completely useful. These fractions are better during Summer and worst during Winter.

We finally conclude that our additional analysis of the astronomical conditions at Calar Alto agree with our previous results presented in Paper I. The new data strength our previous conclusion that it is a good astronomical site, similar in many aspects to places where there are 10m-like telescopes under operation or construction.

For both reasons we consider that this observatory is a good candidate for the location of future large aperture optical/NIR telescopes.

<sup>5</sup> [http://www.cyanogen.com/products/cloud\\_main.htm](http://www.cyanogen.com/products/cloud_main.htm)

## 5. ACKNOWLEDGMENTS

SFS thanks the Spanish Plan Nacional de Astronomía program AYA2005-09413-C02-02, of the Spanish Ministry of Education and Science and the Plan Andaluz de Investigación of Junta de Andalucía as research group

## FQM322.

We acknowledge Dr. M.Moles, PI of the ALHAMBRA survey, for allowing us the access to the data of this project.

## REFERENCES

- Benn, C.R., Ellison, S.L., 1998, La Palma Technical Note, 115.  
 Benn, C. R., & Ellison, S. L. 1998, *New Astronomy Review*, 42, 503  
 Birkle, K., Elsasser, H., Neckel, T., Schnur, G., & Schwarze, B. 1976, *A&A*, 46, 397  
 “Results from the Eso Large Program on Transneptunian Objects and Centaurs”, Boehnhardt et al., *Earth, Moon and Planets*, Volume 92, Numbers 1-4, June, 2003  
 Casali M.M., & Hawarden T.G., 1992, *UKIRT Newsletter*, 4, 33  
 Chamberlain, J. W. 1961, *International Geophysics Series*, New York: Academic Press, 1961,  
 Content, R. 1996, *ApJ*, 464, 412  
 Cox, A. N. 2000, *Allen’s astrophysical quantities*, 4th ed. Publisher: New York: AIP Press; Springer, 2000. Edited by Arthur N. Cox. ISBN: 0387987460,  
 Cuby J., et al., 2000, *The Messenger* 101, 3  
 Glass, I. S. 1999, *Highlights of Astronomy*,  
 Harwit, M., Fuhrmann, K., & Werner, M. 1969, *Royal Society of London Philosophical Transactions Series A*, 264, 273  
 Herbst, T. M., Beckwith, S. V., Birk, C., Hippler, S., McCaughrean, M. J., Mannucci, F., & Wolf, J. 1993, *Proc. SPIE*, 1946, 605  
 Hopp, U., Fernández M., 2002, *Calar Alto Newsletter* n.4, <http://www.caha.es/newsletter/news02a/hopp/paper.pdf>  
 Kervella et al. 2006, *A&A*, 459, 669  
 Kovács, Z. 2006, *Publications of the Astronomy Department of the Eotvos Lorand University*, 17, 161  
 Leinert, C., Vaisanen, P., Mattila, K., & Lehtinen, K. 1995, *A&AS*, 112, 99  
 Leinert, C., et al. 1998, *A&AS*, 127, 1  
 Maihara, T., Iwamuro, F., Yamashita, T., Hall, D. N. B., Cowie, L. L., Tokunaga, A. T., & Pickles, A. 1993, *PASP*, 105, 940  
 Moles, M., et al. 2008, *AJ*, 136, 1325  
 Oliva, E., & Origlia, L. 1992, *A&A*, 254, 466  
 Patat, F. 2003, *A&A*, 400, 1183  
 Rousselot, P., Lidman, C., Cuby, J.-G., Moreels, G., & Monnet, G. 2000, *A&A*, 354, 1134  
 Sánchez, S. F., Aceituno, J., Thiele, U., Pérez-Ramírez, D., & Alves, J. 2007, *PASP*, 119, 1186  
 Sarazin, M., & Roddier, F. 1990, *A&A*, 227, 294  
 Skrutskie, M. F., et al. 2006, *AJ*, 131, 1163  
 Tody, D. 1993, “IRAF in the Nineties” in *Astronomical Data Analysis Software and Systems II*, A.S.P. Conference Ser., Vol 52, eds. R.J. Hanisch, R.J.V. Brissenden, & J. Barnes, 173.  
 Ziad, A., et al. 2005, *MNRAS*, 362, 455

TABLE 1  
LOG OF THE DATA-SET PER NIGHT

Date(s)	Telescope	Instrument	Bands	Number of frames
30/01/08	1.23m	Magic	J,H,Ks,K,Km	24 per band
31/01/08	1.23m	Magic	J,H,Ks,K,Km	24 per band
ALHAMBRA(1)	3.5m	Omega2000	J,H,Ks	17
ALHAMBRA(2)	3.5m	Omega2000	J,H,Ks	1954,2394,2963

- (1) 7 nights of observations in August 2004 from the ALHAMBRA survey. Analysis based on the reduced and combined frames.  
(2) 75 nights of observations between August 2004 and March 2008 from the ALHAMBRA survey. Analysis based on the individual frames.

TABLE 2  
TYPICAL VALUES OF THE NIGHT-SKY SURFACE BRIGHTNESS AT CALAR ALTO IN THE NIR

Description	J	H	Ks	K	Km
Calar Alto, 1.23m Telescope, MAGIC, 30/01/08					
median	16.45	14.36	12.57	11.97	12.78
brightest	16.18	14.18	11.49	11.88	12.69
darkest	16.69	14.54	12.73	12.15	12.88
Calar Alto, 1.23m Telescope, MAGIC, 31/01/08					
median	15.53	14.03	12.54	12.02	12.76
brightest	14.91	13.39	12.38	11.81	12.54
darkest	16.52	14.98	12.82	12.34	13.04
Calar Alto, 3.5m Telescope, Omega2000, ALHAMBRA, August 2004					
median	16.04	14.04	12.20	–	–
brightest	15.45	13.45	11.93	–	–
darkest	16.57	14.80	12.70	–	–
Calar Alto, 3.5m Telescope, Omega2000, ALHAMBRA, Full sample					
median	15.64	13.76	12.28	–	–
darkest	16.96	14.98	13.55	–	–

TABLE 3  
THE NIGHT-SKY SURFACE BRIGHTNESS AT CALAR ALTO IN THE NIR AT THE ZENITH

Description	J	H	Ks
Airmass<1.05	15.92	13.88	12.49
Airmass corrected	15.95	13.99	12.39
Winter	15.92	13.99	12.89
Summer	15.97	14.02	12.07

TABLE 4  
THE NIGHT-SKY SURFACE BRIGHTNESS IN OTHER OBSERVATORIES

Description	Height (m)	Type	J	H	Ks	Reference
La Palma	2500	Average	15.5	14.0	12.6	1 & 2
Paranal	2635	Darkest	16.5	14.4	13.0	3 & J.Cuby et al. (2000)
		“ Darkest	–	–	13.2	Kervella et al. (2006)
		“ Darkest	–	–	13.5	Boehnhardt et al. (2003)
Cerro Pachon	2200	?	16.0	13.9	13.5	4
Mt.Graham	1926	?	–	–	13.5	5
Mauna Kea	4200	Darkest	16.75	14.75	14.75	6
		“ Average	15.6	14.0	13.4	7
Mt.Hamilton	1283	?	16.0	14.0	13.0	8
Kitt Peak	2096	?	15.7	13.9	13.1	9
Anglo Australian Obs.	1164	?	15.7	14.1	13.5	10

- (1) F. Ghinassi: <http://www.tng.iac.es/instruments/nics/imaging.html#zpoints>
- (2) M.Pedani: [http://www.tng.iac.es/info/la\\_palma\\_sky.html](http://www.tng.iac.es/info/la_palma_sky.html)
- (3) <http://www.eso.org/genfac/pubs/astclim/paranal/skybackground/>
- (4) <http://gemini.fcaglp.unlp.edu.ar/sciops/ObsProcess/obsConstraints/obsConstraints.html>
- (5) [http://www.bo.astro.it/~cilegi/astro/nirvana/DOCUMENTS/doc\\_nirvana\\_V1.2.pdf](http://www.bo.astro.it/~cilegi/astro/nirvana/DOCUMENTS/doc_nirvana_V1.2.pdf)
- (6) <http://www.jach.hawaii.edu/UKIRT/astronomy/sky/skies.html>
- (7) <http://casu.ast.cam.ac.uk/surveysprojects/wfcam>
- (8) [http://mthamilton.ucolick.org/techdocs/instruments/ircal/ircal\\_detector.html](http://mthamilton.ucolick.org/techdocs/instruments/ircal/ircal_detector.html)
- (9) <http://www.noao.edu/kpno/manuals/flmn/flmn.html>
- (10) [http://www.aao.gov.au/AAO/iris2/iris2\\_overview.html#Imaging\\_sensitivities](http://www.aao.gov.au/AAO/iris2/iris2_overview.html#Imaging_sensitivities)

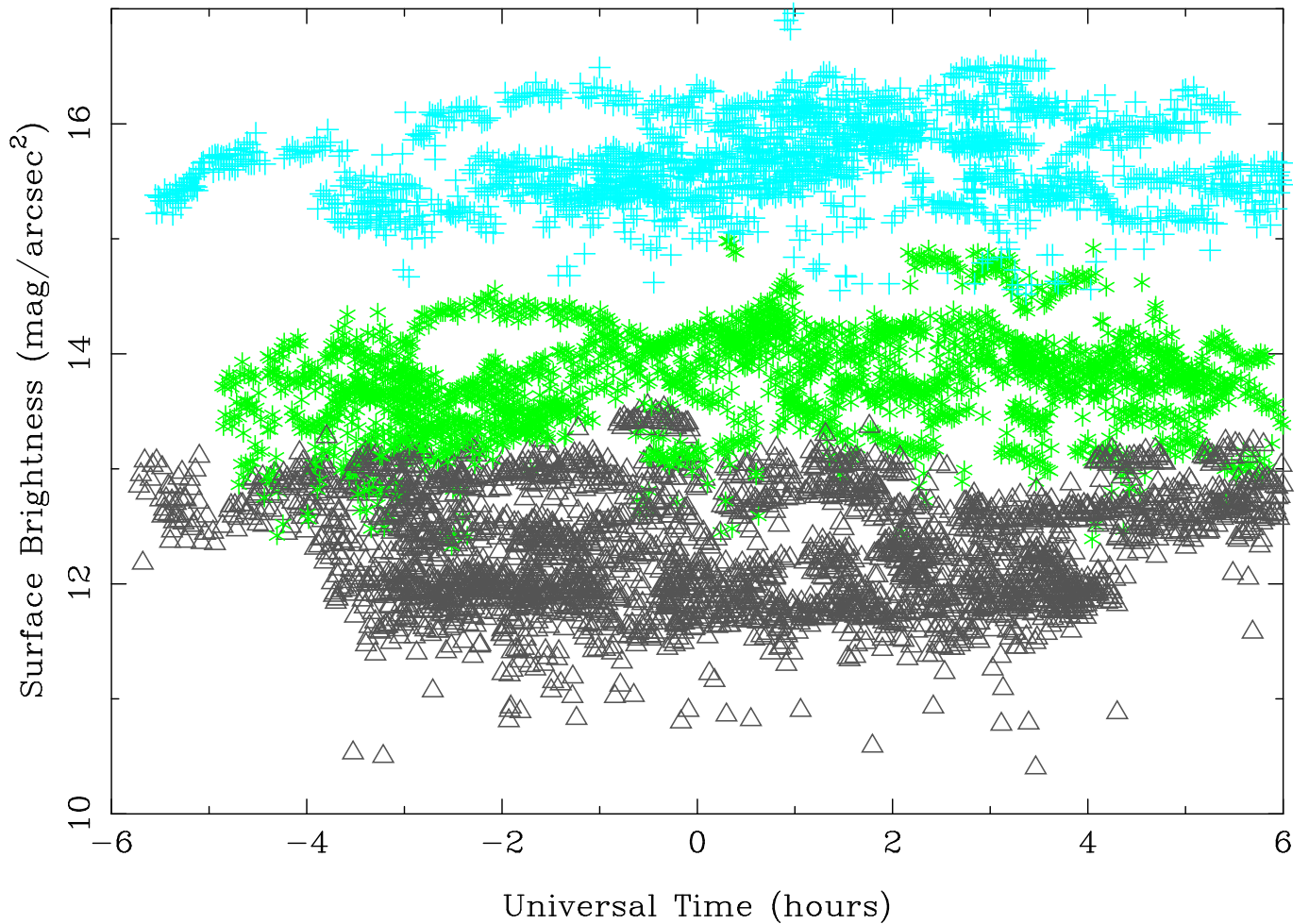


FIG. 1.— Distribution of the NIR surface sky brightness in different bands, derived using the data from the ALHAMBRA survey, along the Universal Time, for the 75 nights covered by our dataset, expanding from August 2004 to March 2008. The plot shows 1954, 2394 and 2963 individual points for the  $J$ ,  $H$  and  $K_s$  bands, respectively. Blue crosses represent the values for the  $J$ -band, green stars represent the values for the  $H$ -band, and gray triangles represent the values for the  $K_s$ -band. The range of night sky surface brightnesses for each band are clearly appreciated.

31/01/08

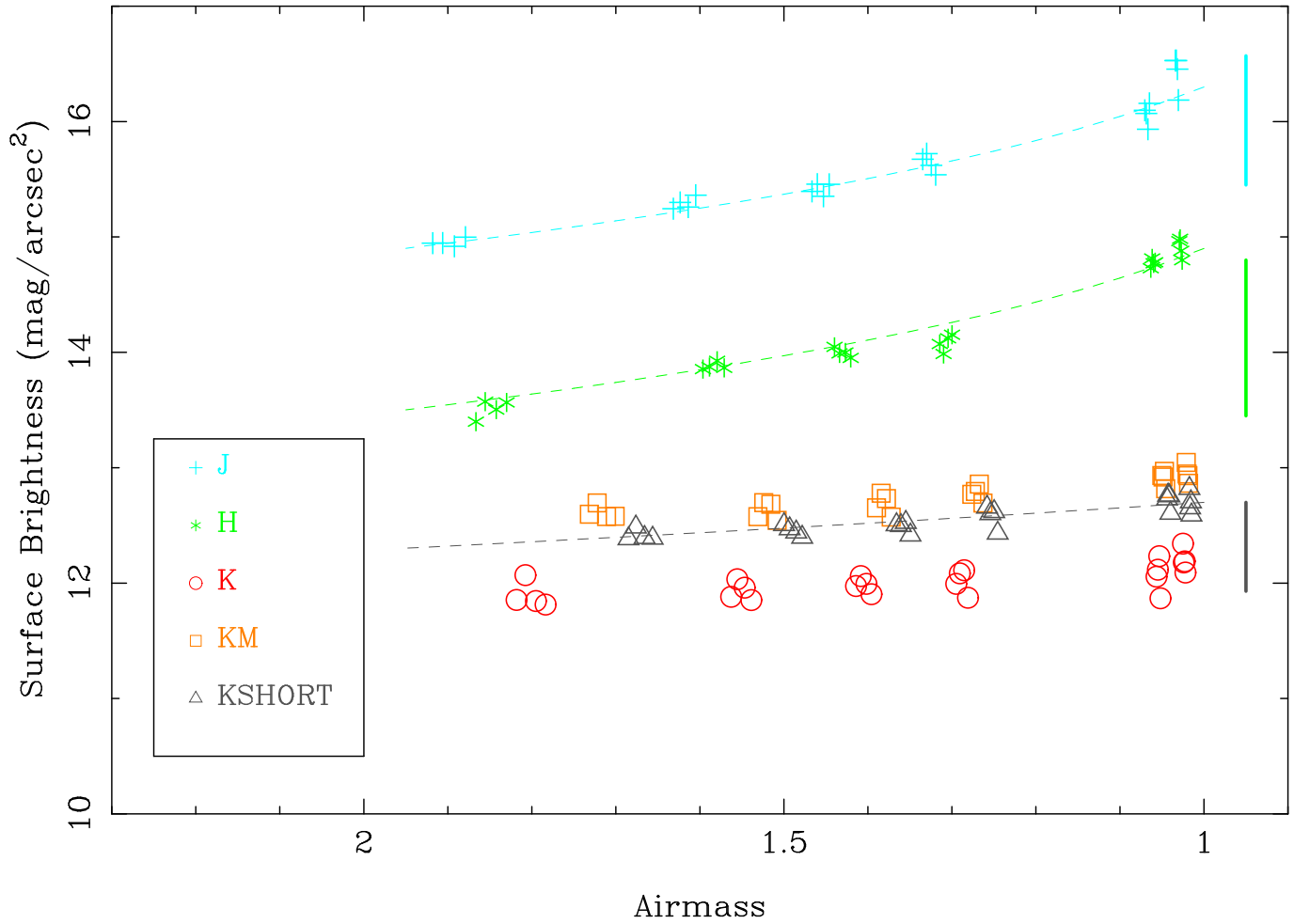


FIG. 2.— Distribution of the NIR surface sky brightness in different bands along the airmass for the night of the 31st of January 2008. The symbols for the different bands are described in the plot. There is clear dependency of the surface brightness with the airmass, particularly strong in the J and H bands. This dependency can be reproduced assuming an increase of the background flux with the airmass as it can be seen with the corresponding overplotted lines. A similar distribution is appreciated in all nights from our dataset.

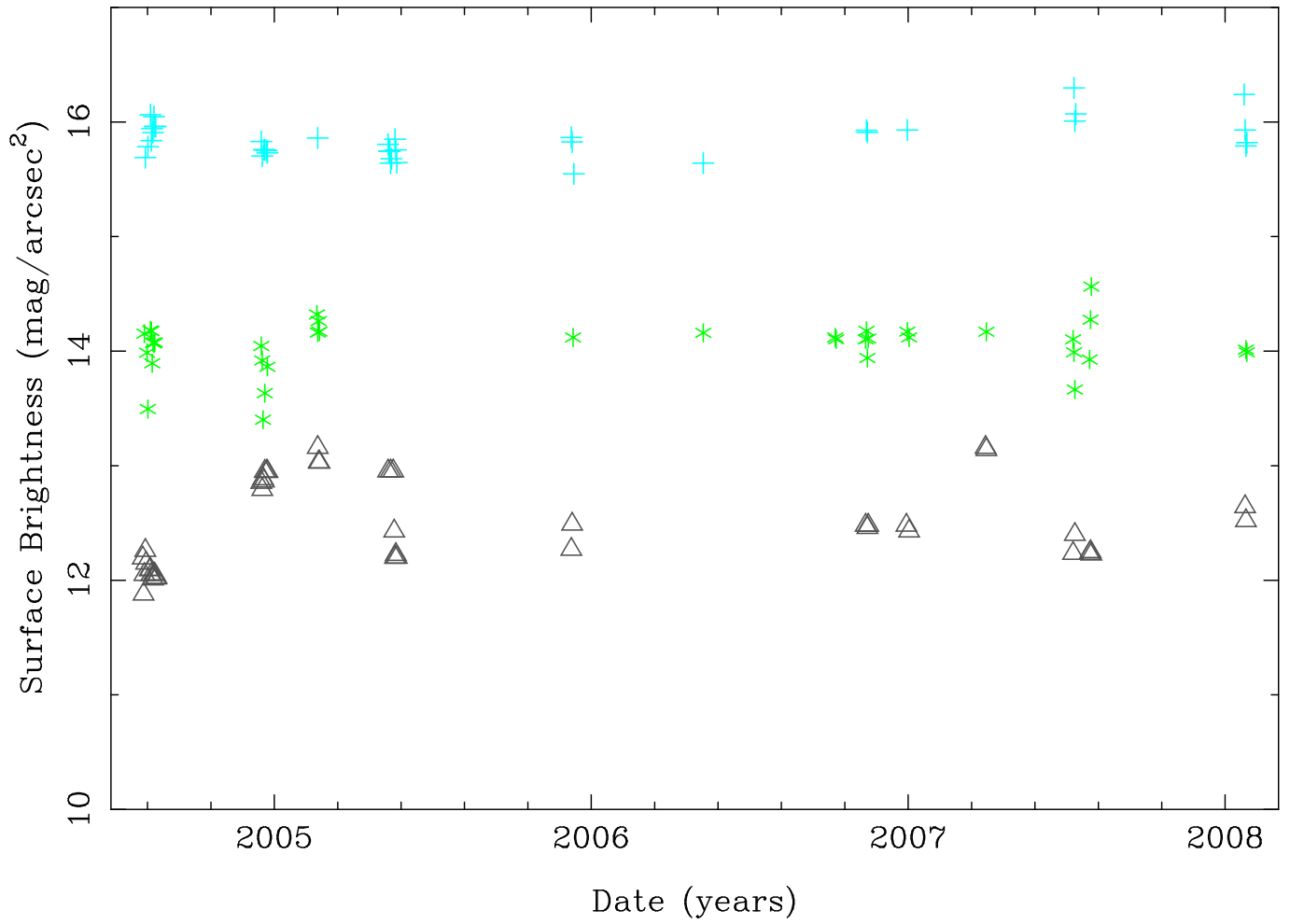


FIG. 3.— Distribution of the air-mass corrected NIR surface sky brightness for the J, H and Ks bands, averaged for each night, along the time. The symbols for each band are similar to those of the figure 2. There is a clear seasonal trend in the Ks band, being the sky brighter in summer than in winter.

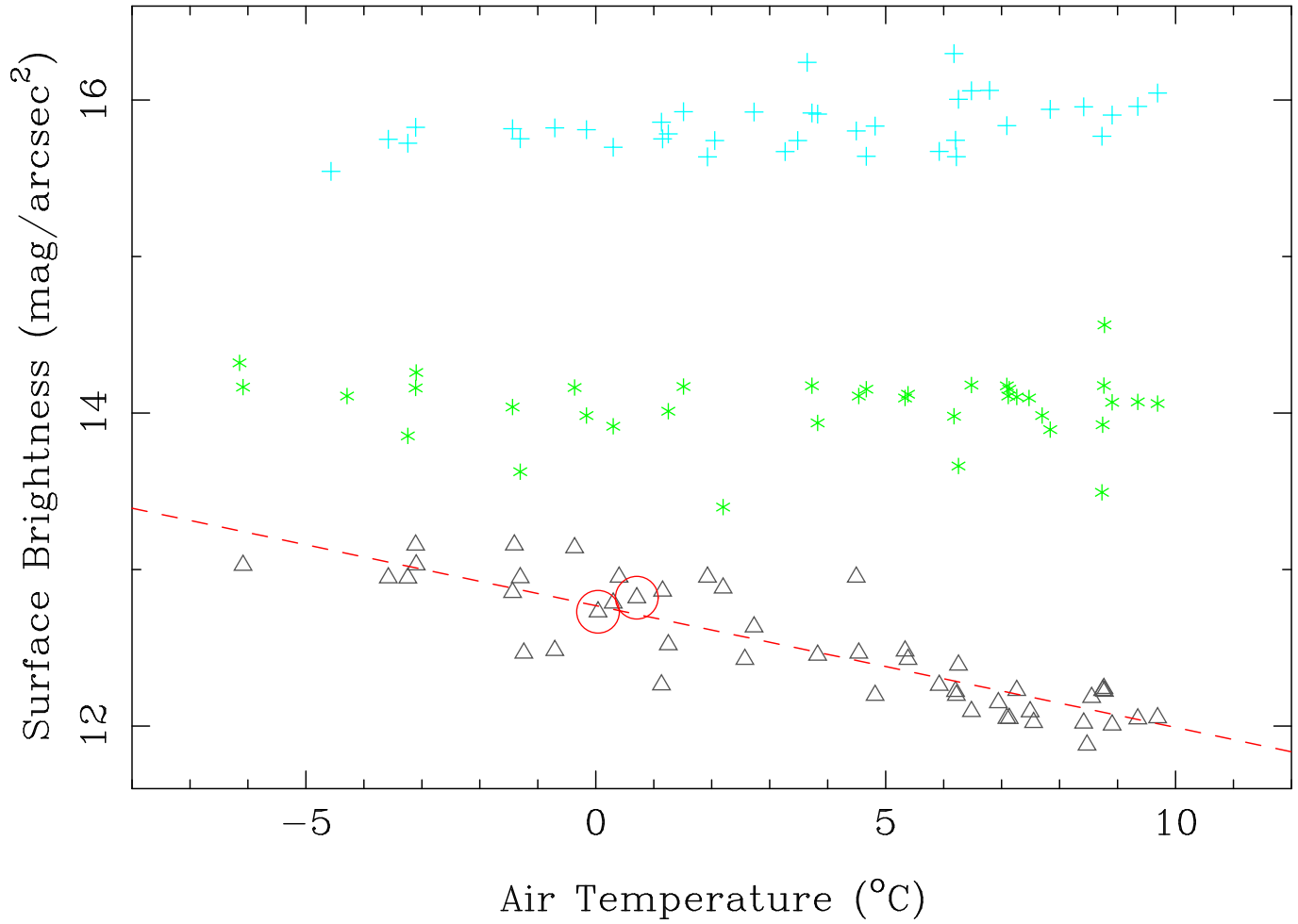


FIG. 4.— Distribution of the airmass corrected surface sky brightness for the  $J$ ,  $H$  and  $Ks$  bands, averaged for each night, along the average night temperature. Only for the  $Ks$ -band a clear correlation between both parameters is seen. The dashed line represent the best linear regression fit over the  $Ks$ -band data. The encircle data indicate the data taken with the 1.23m Telescope.

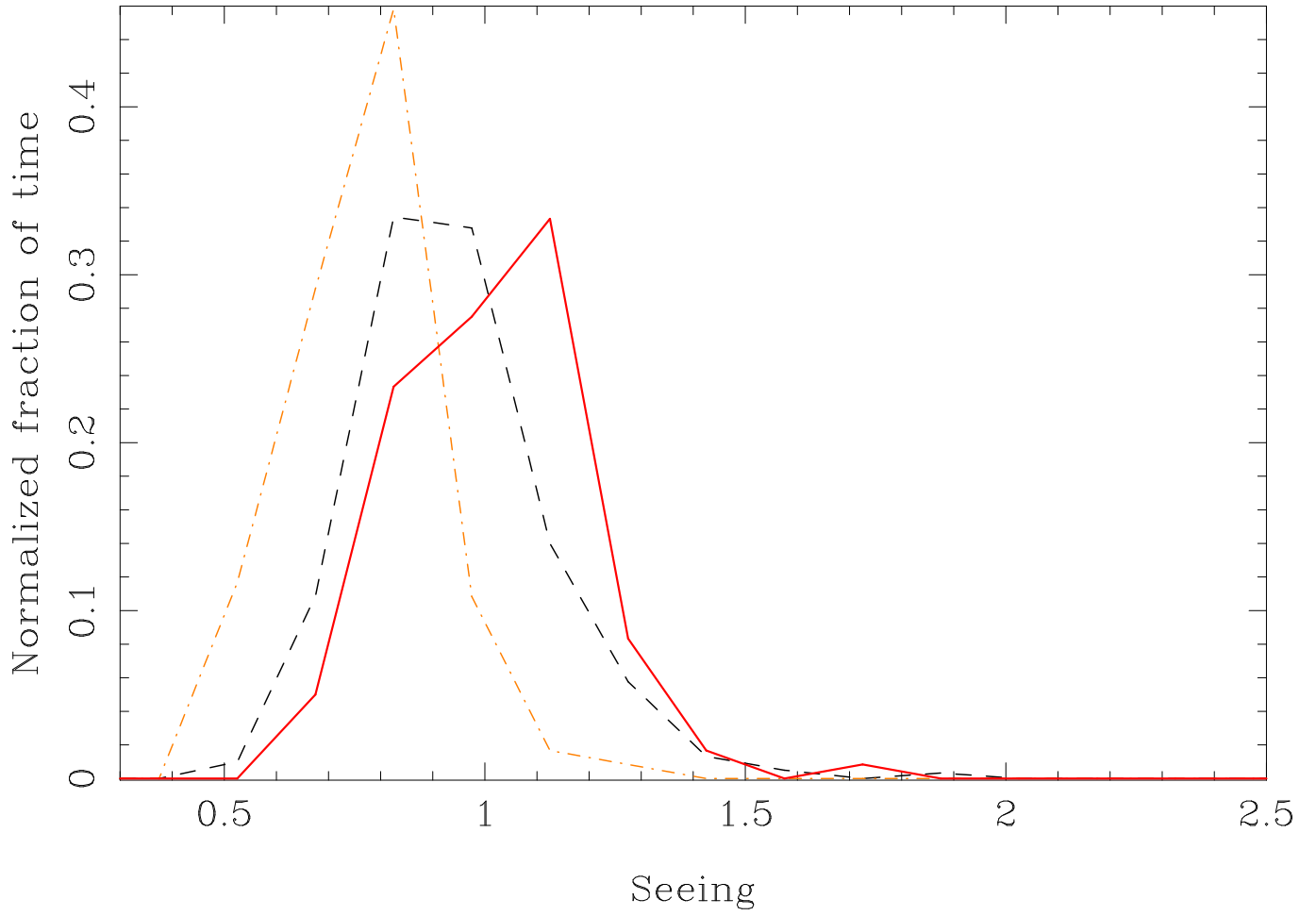


FIG. 5.— Distribution of the telescope seeing at the V-band derived from the analysis of the 7311 NIR individual images from the ALHAMBRA survey (red solid line) corresponding to the time period between August 2004 and March 2008, compared with a similar distribution of the atmospheric seeing, derived from the DIMM monitor in the same time period (black dashed line). The orange dash-dotted line shows the distribution of the original seeing measured in the  $Ks$ -band images.

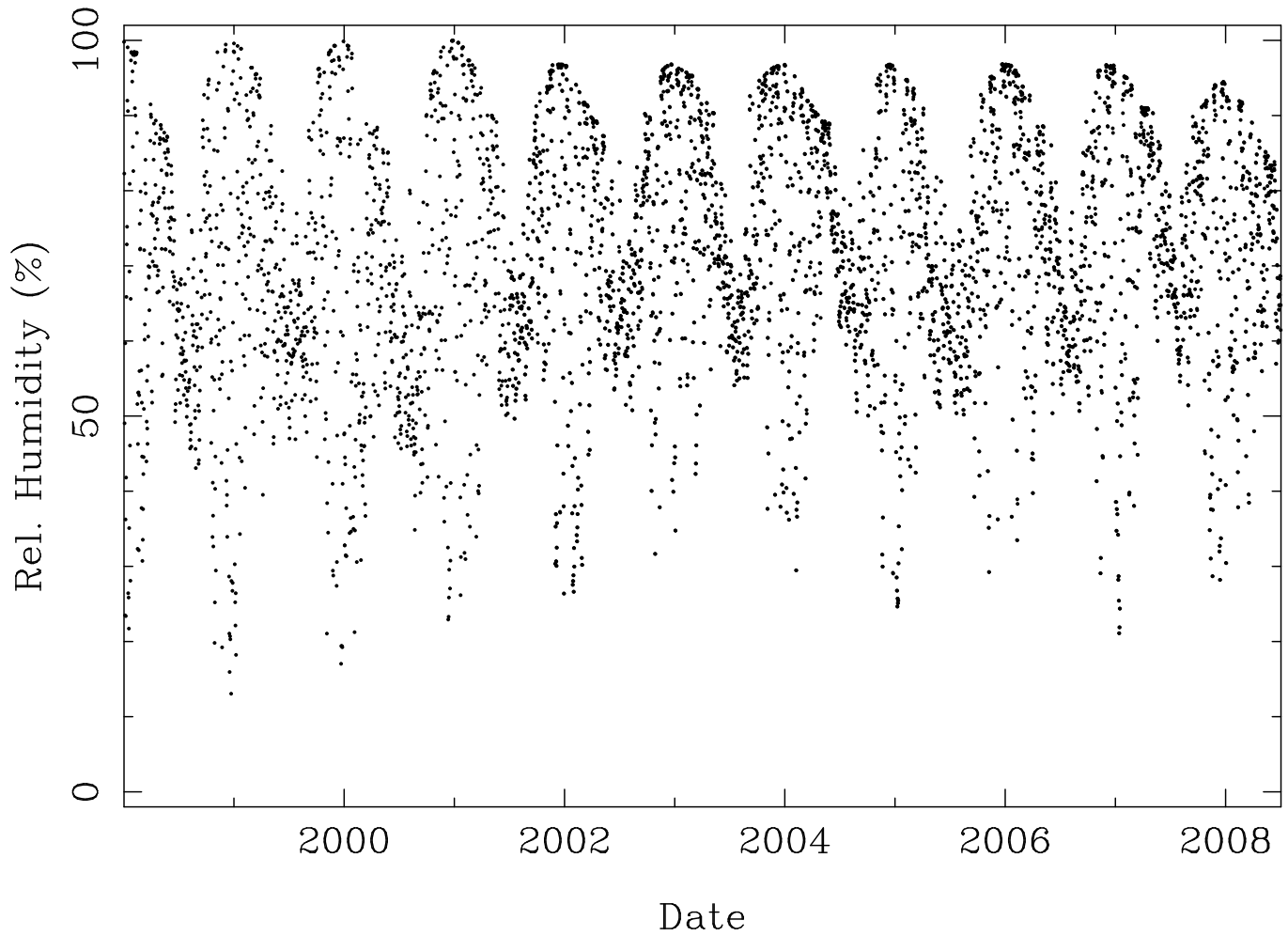


FIG. 6.— Distribution of the average relative humidity per night along the time period between January 1998 and December 2007. There is a clear seasonal pattern, with the relative humidity being more frequently higher and more instable in winter than in summer. The driest periods are also shown in winter, associated with freezing temperatures.